Research on Engineering Structures & Materials
www.jresm.org
Research Group

Research Article

Numerical investigation on the compressive behavior of solid TPMS lattices designed for 3D concrete printing

Asmae Najm-Eddine [*,1,a], Ismail Arroub [1,b], Ahmed Bahlaoui [1,c], Mohamed Abouelmajd [2,d], Youssef Najm-Eddine [1,e], Ilham Erritali [3,f], Abdelhak Daiz [1,g], Ismail Ezzaraa [4,h], Soufiane Belhouideg [4,i]

[1]*Team of Research in Energetics, Renewable Energies and Materials, Sultan Moulay Slimane University, Faculty of Applied Sciences, Beni Mellal, Morocco*
[2]*FEMTO-ST Institute, CNRS, Marie et Louis Pasteur University, Besançon, France*
[3]*Industrial Engineering and Surface Engineering Laboratory, Faculty of Science and Technology, Sultan Moulay Slimane University, Beni Mellal, Morocco*
[4]*Research Laboratory in Advanced Sciences and Technologies (LRSTA), National School of Applied Sciences, Sultan Moulay Slimane University, Beni Mellal, Morocco*

Article Info

Article History:

Received 02 Feb 2026

Accepted 05 Oct 2026

Keywords:

Numerical investigation;
3D concrete printing;
Light-weighting;
Mechanical behavior;
TPMS lattices

Abstract

Lightweight cellular structures with customized geometries and mechanical properties can be effectively designed using Triply Periodic Minimal Surface (TPMS) lattices. Their continuous, periodic nature makes them especially well-suited for numerical analysis of the relationships among topology, relative density, and mechanical response. In this study, a finite element (FE) framework was first validated against experimental compression data reported in the literature for 3D printed Ultra-High-Performance Fiber-Reinforced Concrete (UHPFRC) octet-truss lattice specimens (50.8 × 50.8 × 203.2 mm) with strut diameters of 8, 10, and 11 mm and relative densities of 33.6%, 46.6%, and 52.5%, respectively. The FE model was validated and subsequently employed to numerically investigate the compressive behavior of three UHPFRC solid TPMS lattice topologies, namely Primitive, Neovius, and I-Wrapped Package (I-WP), at a relative density of 40%. The simulation results demonstrated marked variations in mechanical behavior among the investigated topologies, with ultimate compressive strengths ranging from 5 MPa to 62 MPa and Young's modulus values from 183 MPa to 513 MPa, highlighting the effects of topology and material layout on stiffness and load-carrying capacity. These findings provide insight into the structural performance of TPMS-based UHPFRC lattices and highlight their potential for future additive manufacturing and 3D concrete printing applications. However, the manufacturability and printability of the proposed TPMS geometries were not investigated and remain subjects for future experimental work.

© 2026 MIM Research Group. All rights reserved.

1. Introduction

Three-dimensional concrete printing (3DCP) is an emerging layer-by-layer construction technique that enables the production of cement-based parts with complex forms and dimensional accuracy, eliminating the need for conventional formwork [1]. The introduction of ultra-high-performance fiber-reinforced concrete (UHPFRC) in digital concrete has marked a major progression in the digital manufacturing of cementitious materials. Although UHPFRC has good mechanical properties, its use in 3D printing is limited due to poor rheological properties and printability.

*Corresponding author: najmeddine.asmae.fpb21@usms.ac.ma
[a]orcid.org/0000-0009-3739-7711; [b]orcid.org/0000-0003-4263-2877; [c]orcid.org/0000-0009-7457-3921; [d]orcid.org/0000-0002-1035-3980; [e]orcid.org/0000-0008-1476-0023; [f]orcid.org/0000-0002-8093-8263; [g]orcid.org/0000-0000-2737-0499; [h]orcid.org/0000-0003-0654-030X; [i]orcid.org/0000-0003-2949-8618
DOI: http://dx.doi.org/10.17515/resm2026-1490st0202rs

Recent studies [2–6] have therefore aimed to optimize mix design parameters, including fiber distribution and the use of superplasticizers, to ensure buildability and interlayer bonding in printed elements. The changes to the mix designs improve interlayer adhesion and geometric accuracy in the printed structures. Thus, UHPFRC for digital fabrication offers improved mechanical properties and design possibilities for future construction. One of the important developments in the field of 3DCP is the concept of lightweighting, where the structural efficiency of the structure is enhanced by reducing the amount of material and self-weight, without compromising the ability to carry and withstand loads. The objective of lightweighting is achieved through the utilization of triply periodic minimal surface lattice structures, in which the curvatures of the lattice are locally balanced to zero, the lattice has no edges, and the pores are interconnected. Furthermore, the lattice structure allows for uniform adjustment of pore width. Additionally, the lattice structure has high porosity and high surface area. The aforementioned lattice structures, including the Diamond, Gyroid, and Schwarz lattices, show higher specific strength and stiffness due to evenly distributed stress and a high surface-to-volume ratio. The lattice structure, when used in 3D-printed concrete structures, enables customized mechanical properties, reduced material use, and enhanced sustainability.

By combining high specific strength, structural light-weighting, and controlled energy absorption, UHPFRC solid TPMS lattices present substantial deployment potential for modern construction. Key potential engineering applications include precast lightweight floor core panels, protective impact barriers, energy-absorbing crash cushions, and topologically optimized structural nodes for digital construction. Several studies have explored the construction of additively manufactured concrete lattice structures. In his study, Wang et al. [7] explored the use of hollow inner structures (such as cellular, truss-like, or lattice-shaped) in 3D-printed components. At the same time, [8] presented a strategy for numerically simulating 3D-printed lattice structures to predict their behavior, and Hu et al. [9] found that multi-scale porous structures, such as those composed of triply periodic minimum surfaces (TPMS), could enhance performance with minimal weight. Different researchers have examined the structural integrity of TPMS structures by using numerical and experimental methods. Chatzigeorgiou et al. studied lattices under tensile and shear loads [10]. In [11-14], the authors explored these structures under flexural tests. A comprehensive analysis of TPMS structures made of different materials has been conducted to assess their potential to improve the properties of concrete structures. Metallic TPMS lattices have gained significant attention, as discussed in [15,16]. The quasi-static and dynamic compressive properties of different metallic TPMS sheet lattices, namely, Primitive, IWP, Gyroid, Fisher-Koch, and Diamond, were thoroughly analyzed in [17]. The mechanical response of functionally graded TPMS lattices was also discussed in [18,19], and those of three polymeric Sheet TPMS cellular structures were evaluated through experimental and numerical modeling in [20]. This research revealed that the Neovius and I-WP structures behave similarly and outperform the primitive structure in terms of stiffness and strength. Further studies on PLA TPMS lattices were conducted and reported in [21-23]. The compressive properties of foamed-concrete TPMS lattices were also evaluated in [24], whereas the use of metallic TPMS lattices to reinforce UHPFRC was discussed in [25]. Furthermore, the integration of 3D-printed ABS resin TPMS lattices into a cementitious matrix was investigated in [14]. The influence of combining two different TPMS lattice types on mechanical behavior was analyzed in [26].

While the architectures of Triply Periodic Minimal Surfaces (TPMS) have been thoroughly studied in both polymeric and metallic materials, there is a lack of research on solid TPMS structures made from Ultra-High-Performance Fiber-Reinforced Concrete (UHPFRC). Additionally, a systematic comparison of the mechanical performance of the most commonly used solid TPMS topologies: Primitive, Neovius, and I-WP has not been conducted for UHPFRC-based structures. As a result, the impact of topology on the structural efficiency of lightweight load-bearing UHPFRC components is not well understood. To address this gap, the present study conducts a systematic numerical investigation of three solid TPMS geometries using a finite element model validated against published experimental data. The objective of this computational analysis is to evaluate and compare the mechanical efficiency of Primitive, Neovius, and I-WP UHPFRC lattices under compressive loading. To isolate the influence of topology, all structures were simulated at a

constant relative density of 40%. This was done to achieve a stable structure without making its members too thin and susceptible to buckling.

The sections can be organized as follows: the FE model's validation process and numerical modeling are explained in Section 2. The numerical simulations' results are discussed in Section 3. The weaknesses of the FE model are described in Section 4. Concluding remarks are stated in Section 5.

2. Materials and Methods

2.1 Validation of the FE Model

This section highlights the procedure followed for FE model verification using compression tests conducted on samples described in [27]. The reference samples consisted of UHPFRC octet-truss lattice structures measuring 50.8×50.8×203.2 mm with strut diameters of 8 mm, 10 mm, and 11 mm, respectively. Relative density values for these samples are 33.6%, 46.6%, and 52.5%, respectively, as depicted in Fig. 1 below. The specimens underwent the same uniaxial compression testing, and the same UHPFRC material properties that were documented in [27], as illustrated in Table 1 and Fig. 2.

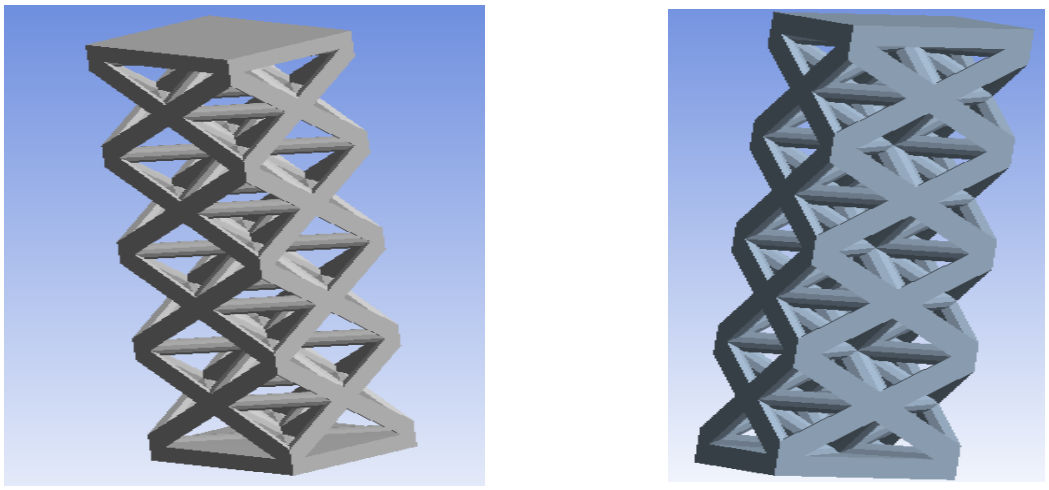


Fig. 1. 8 mm and 10 mm diameter octet truss lattices

Table 1. Mechanical properties of UHPFRC [27]

Young's modulus (MPa)	Poisson's ratio	Density (Kg/m3)	Ultimate compressive stress (MPa)	Yield stress (MPa)	Tensile yield stress (MPa)	Tensile ultimate strength (MPa)
30000	0.18	2300	144	138	6	10

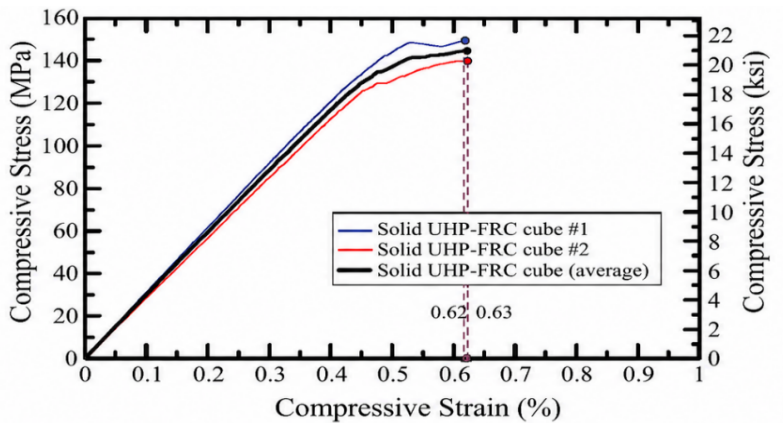


Fig. 2. Stress-strain curves of UHPFRC [27]

The objective of this validation is to evaluate the accuracy and reliability of the FE modeling framework before applying it to the numerical investigation of the topologically optimized TPMS lattice structures. The continuum model is based on the assumption of isotropic multilinear plastic deformation derived from digitized uniaxial compression stress-strain test data as reported in Table 2. Micro-cracking, concrete crushing, and fiber alignment have been deliberately avoided to study the effect of global structure topology under large deformation settings. Numerical simulations were performed using the Static Structural module of ANSYS Workbench, with the validation model discretized using 0.1 mm 10-node 3D quadratic tetrahedral solid elements (solid187). The multilinear stress–strain curve was digitized directly from the experimental UHPFRC compressive test data reported in [27] (Fig. 2), with an initial linear-elastic limit at a yield stress of 138 MPa and a peak compressive stress of 144 MPa. The tensile strength was included in the ANSYS material definition as a supplementary material property required for the numerical formulation; however, the tensile behavior of UHPFRC was not investigated in the present study. The material response was therefore governed by the prescribed elastic-plastic constitutive data rather than by an independent numerical fracture criterion. Axial loading was applied under large-deformation conditions by imposing a displacement equivalent to 10% compressive strain on the top surface over a 100-second simulation. In contrast, the bottom surface was constrained in the loading direction. The loading plates were modeled as rigid bodies, as in the experimental test; metallic plates were used, and their stiffness was significantly greater than that of the lattice specimen. The upper and the bottom plates were simulated as bonded to the specimen. Load transfer occurred through these contact interfaces, enabling the compressive load to be transmitted from the upper plate to the lattice and then to the lower plate. Fig. 3 illustrates the loading and boundary conditions adopted in our simulation. Since 3D solid elements (SOLID187) possess only translational degrees of freedom at their nodes, rotational restraints were naturally enforced through the fixed translational constraints of the rigid contact surfaces. The apparent Young's modulus of the lattice structure, Eapp, is given in Eq. (1):

$$E_{app} = \frac{Frl}{S\Delta l} \tag{1}$$

Where Fr: reaction force at the top plate boundary; l: initial height of the lattice beam (203.2 mm); S: surface area of the top plate; and Δl: displacement at the top plate surface in the loading direction. The observed Young's Modulus values were calculated for three different diameters of 8, 10, and 11mm.

Table 2. ANSYS multilinear isotropic hardening input

Stress (MPa)	Plastic strain (%)
138	0
140	0.043
141	0.065
142	0.087
143	0.110
144	0.130

Table 3 contains the calculated and experimental results. The magnitude of stress at which the stress-strain curve transitions from its linear elastic portion to its nonlinear portion is defined as the yield strength in this paper. The great degree of agreement between the numerical and experimental results for the octet-truss geometry (see Fig. 4) demonstrates the precision and dependability of the boundary condition assumptions, constitutive material parameters, and finite element model utilized in this investigation. It should be mentioned that this study's validation procedure cannot be regarded as a direct validation of TPMS lattices, but rather establishes confidence in the capability of the numerical modeling approach to predict the compressive behavior of UHPFRC cellular geometries prior to its application to solid TPMS topologies.

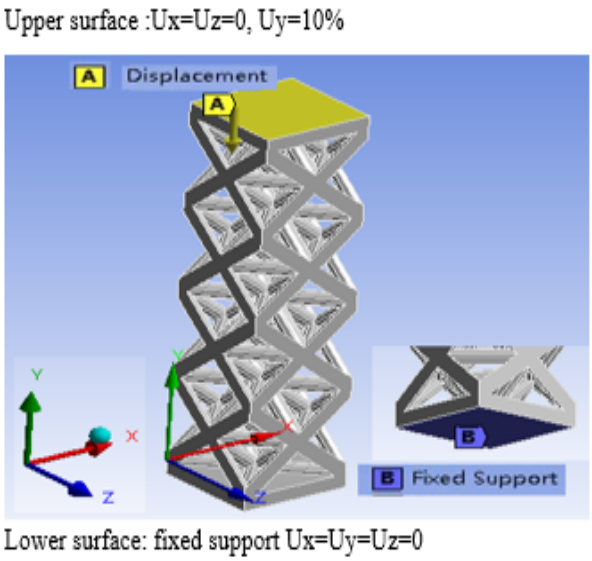


Fig. 3. Boundary conditions and normal applied strain

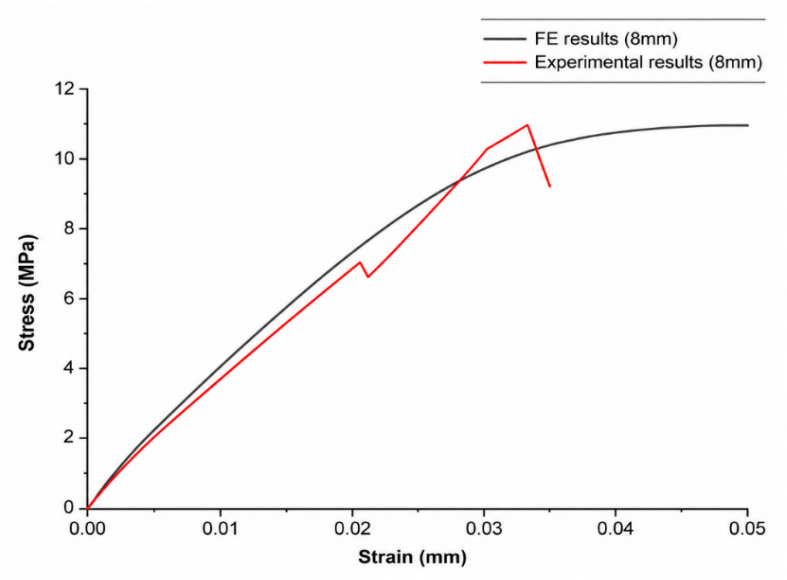
Table 3. Comparison of the numerical findings and the experimental data

Young's modulus (MPa)				Ultimate strength (MPa)		
Diameter (mm)	Empirical values	Simulation results	Relative error (%)	Empirical values	Simulation results	Relative error (%)
8	346.00	355.17	2.65	10.65	10.90	2.35
10	348.50	362.84	4.11	14.08	14.59	3.62
11	357.30	372.41	4.22	18.23	18.97	4.06

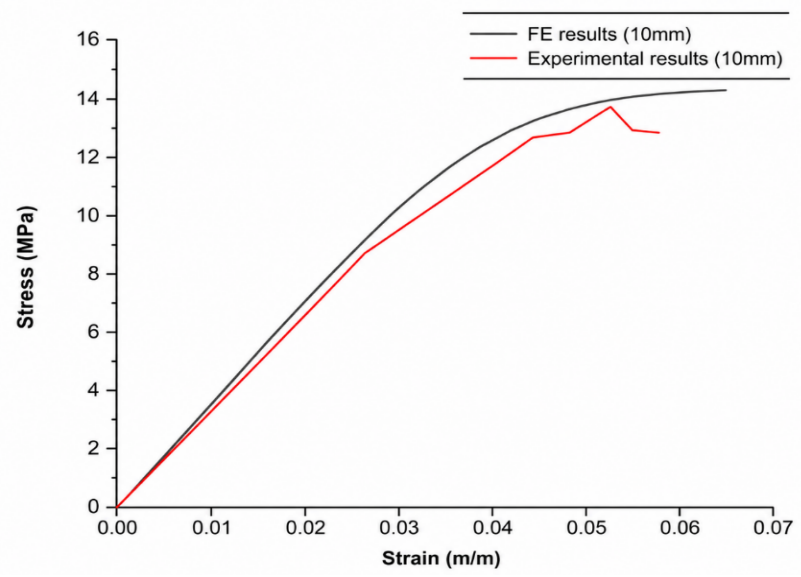
The relative error for the ultimate strength increases from 2.65% to 4.22%, as the relative density rises from 33.6% to 52.5%, which is acceptable for validating our simulation. This behavior is explained by discrepancies between the imperfect materials used in compression tests and the simplified assumptions in FEM models. We observe that the relative error increases as the bulk density ratio of the layered lattice structure rises; the same trend was reported by [28]. This is due to additional imperfections that arise when printing larger concrete lattices, making the structure more susceptible to deformation and failure during the experimental test.

2.2 Numerical Setup

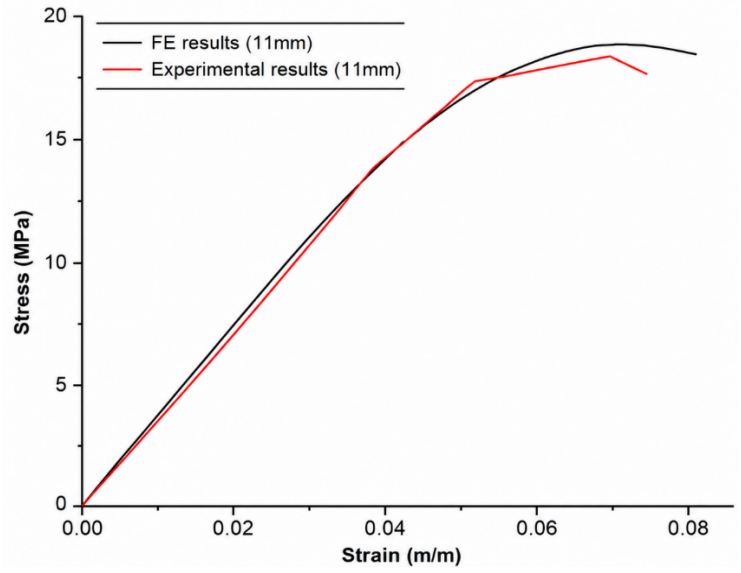
Numerical analysis enables virtual evaluation of material characteristics and the effects of geometric arrangement on mechanical efficiency. Three UHPFRC solid TPMS lattices (Fig. 5), namely Primitive, Neovius, and I-WP, which are mostly studied for their mechanical properties, were simulated under the same boundary conditions as in the validation process to assess the impact of TPMS geometry on the stress-strain curves of these UHPFRC structures. These geometries were generated using MsLattice software at a fixed relative density (ρ^*) of 40%. This specific density was selected as the ideal design criterion because it ensures sufficient structural thickness and stiffness to prevent any premature local buckling under compression, and to ensure the geometry adaptability to 3D concrete printing constraints, and it enables a direct comparison of the three architectures' purely topological efficiency. The STL files were loaded into the Static Structural module of Ansys Workbench, as shown in Fig. 6. Geometries were meshed using the mechanical module and exposed to a 10% strain-equivalent displacement. The simulation time was set to 1000 seconds, and the initial substeps were set to 20. This design measures 50.8 x 50.8 x 203.2 mm, which is the same as the octet truss lattice geometry. A mesh refinement study (Fig. 7) was performed on the I-WP solid lattice geometry to establish numerical convergence and eliminate mesh-sensitivity effects on global stress–strain predictions.



(a)



(b)



(c)

Fig. 4. Comparison of stress-strain curves of experimental and FE results for (a) 8 mm, (b) 10 mm, and (c) 11 mm diameter octet truss lattice

Mesh density was progressively varied from 63058 to 1308801 elements. The convergence indicators were evaluated based on the relative percentage variation in peak compressive stress (σ_u) and apparent Young's modulus (E_{app}) between consecutive refinements. Refining the element size from 0.4 mm (314614 elements) to 0.2 mm (1,308,801 elements) resulted in a change of less than 1.1% in E_{app} and 1.8% in σ_u. In order to achieve the strict condition of convergence at less than 2% deviation, an edge length of 0.4 mm was employed for all TPMS computations going forward.

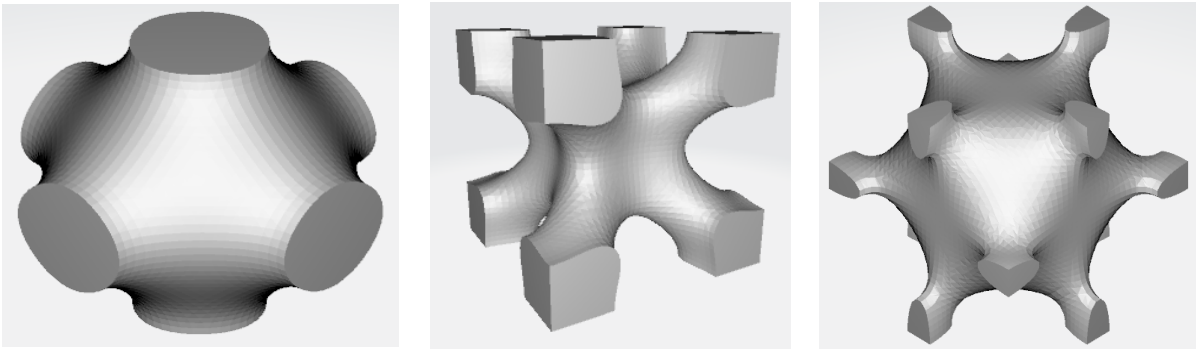


Fig. 5. Primitive (left), I-WP, and Neovius (right) TPMS lattice solid unit cells

3. Results and Discussion

Three TPMS lattices were subjected to a uniaxial compression test, which revealed various mechanical characteristics. For every lattice under investigation, the yield stress and apparent Young's modulus were calculated under the same conditions (10% strain). The Young's modulus, yield strength, and ultimate strength were shown to be significantly positively correlated (see Table 4). This lends credence to the idea that the lattice structure determines the load transmission efficiency. The yield and ultimate strengths increased in proportion to the rise in Young's modulus from 183 MPa (Neovius) to 513 MPa (Primitive). The Gibson–Ashby framework, which anticipates a link between stiffness, strength, relative density, and cellular architecture, is consistent with this relationship. [30]. According to the numerical analysis, under the same relative density ($\rho^* = 40\%$), the unit cell design has a significant impact on the macro-mechanical performance of the UHPFRC TPMS structures. The computational findings show that for the Primitive topology, the alignment of solid material along the loading direction yields an apparent Young's modulus (Eapp = 513 MPa), which is 280% more than Neovius (183 MPa) and 179% greater than I-WP (286 MPa). Furthermore, compared to I-WP (15 MPa) and Neovius (5 MPa), its ultimate compressive strength (σu = 62 MPa) is significantly higher, by factors of 4 and 12, respectively. This demonstrates that under axial compression, the (Primitive) structure with an axial load transfer mechanism offers substantially greater structural efficiency than bending-dominated structures (Neovius).

Despite having the same volume fraction, the TPMS lattice structures under axial loading show contrasting elastic and failure characteristics. According to Fu et al. [29], the TPMS sheet Primitive had a 10% higher compressive strength than the I-WP design. During this simulation, the Primitive solid experienced around 313% more stress than the I-WP design. Similarly, the Primitive solid was almost 1140% more stressed than the Neovius construction (see Table 4), confirming the results of Ahmed et al. [30], who identified the skeletal Primitive geometry as the mechanically most effective TPMS architecture under compressive stress. However, Abueidda et al. [20] found that both Neovius and polymeric I-WP constructions exhibited similar mechanical response and greater stiffness and compressive strength than Primitive design. However, I-WP and Neovius were found to be roughly 277% and 258% stronger mechanically than Primitive, respectively, by Shevchenko et al. [31]. The Primitive arrangement had a larger stress value that corresponded to the maximum strain, indicating a greater capacity for deformation before collapse. The varying relative density values, geometric configurations, and loading circumstances may account for the discrepancy between the results obtained and those reported in the literature. The deformation is influenced by the materials and unit cell size. Although TPMS sheet structures have been extensively studied, the current study focuses on solid UHPFRC TPMS lattices, which may have a different loading mechanism of failure under compression (see Table 5).

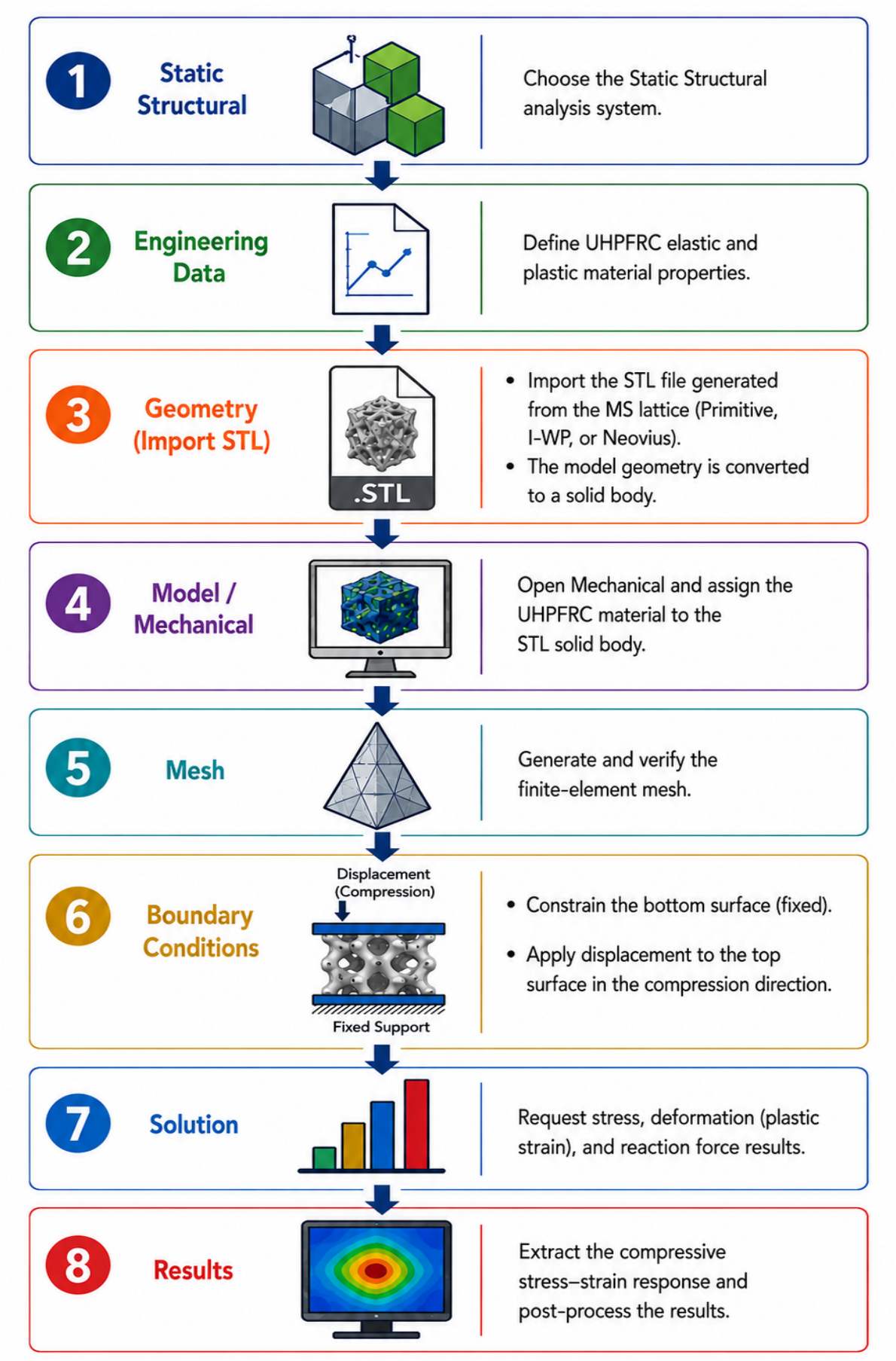


Fig. 6. Numerical workflow for TPMS–UHPFRC compression analysis

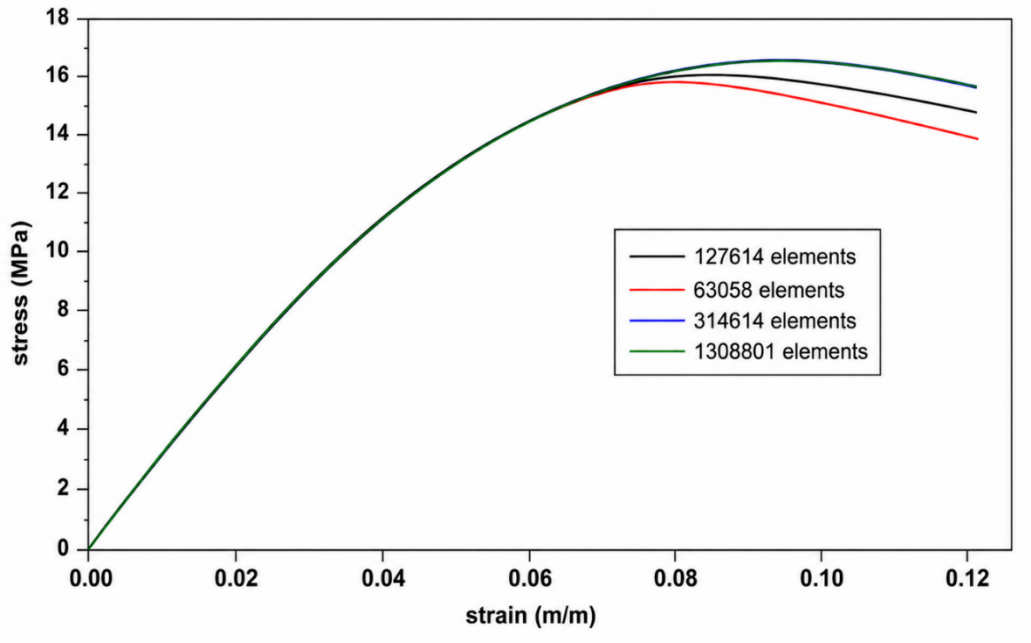


Fig. 7. Mesh convergence analysis

When comparing the primitive, I-WP, and Neovius normal stress concentration zones, each version reveals a distinct stress distribution (Fig. 8). In the primitive lattice, stress is highly localized at the corners, creating continuous vertical load paths through the structure. By contrast, the I-WP lattice exhibits a more distributed stress field, with stressed regions occupying a large portion of the continuous surface and showing less localization. The Neovius lattice shows the most homogeneous stress field, with small, junction-confined local stress regions, and only part of the structure is moderately loaded. Different topology-related mechanisms of deformation are demonstrated by the sequential growth of the von Mises stress concentration zones under compressive loading. In all topologies, the curved nodal fillets produce stresses in the elastic state. Stresses in the Primitive topology increase dramatically in the vertical load channels during the plastic state, resulting in local column junction yielding while leaving nearby regions with modest stress levels. The I-WP and Neovius topologies, on the other hand, cause the structure to yield and bend significantly before failing because the stress concentration zones distribute widely across the doubly curved shell surfaces. The continuous material channels that flow through the structure along the Y-axis, where the primary compressive forces apply, are solely responsible for the primitive solid lattice's superior load-carrying capacity. The Primitive design permits straight, column-like structural pathways that provide maximum axial stiffness (Eapp = 513 MPa), in contrast to the I-WP and Neovius lattices' bending cell structure, which has intricate and winding paths for force transfer. The I-WP and Neovius structures' less concentrated stress patterns result in ineffective force transmission and, thus, lower compressive strength.

The strength ratio used to evaluate the structural efficiency of the three distinct topologies is shown in Table 6. Because of its strength ratio of 3.10, which demonstrates its load sustainability beyond yielding, the Primitive lattice structure is the most effective. However, the I-WP and Neovius lattices showed no rise in stress above yielding, suggesting that their deformation is inadequate.

The Primitive lattice has a wide range of hardening, as demonstrated by the stress-strain graphs in Fig. 9. The Primitive solid TPMS lattice performed better overall, particularly in elasticity, yield strength, and ultimate strength, according to an analysis of the variations in the stress-strain plots of the Primitive, I-WP, and Neovius TPMS lattices (Fig. 9). By enhancing ductility, strain hardening increases the structure's capacity to bend before failing, making it more appropriate for high load-carrying conditions. According to [23] and [29], the primitive lattices exhibit the highest stiffness and strength among the solid TPMS lattices under typical load scenarios.

Table 4. Mechanical characteristics of the three solid TPMS lattices (ρ* = 40%)

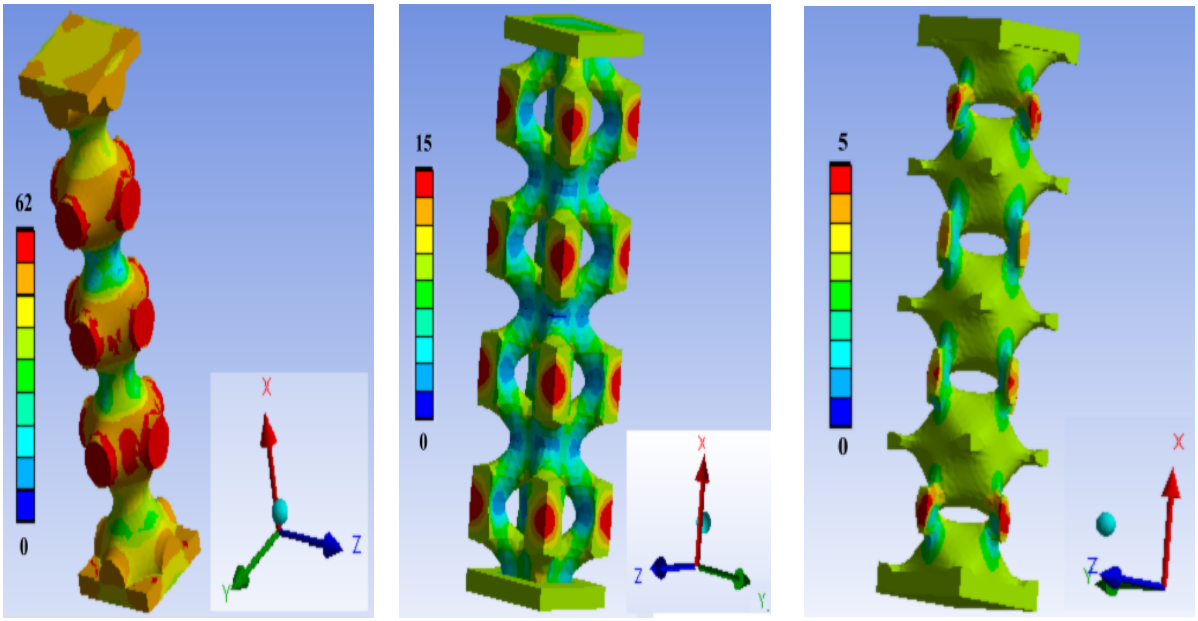
Lattice	Young's Modulus (MPa)	Yield Strength (MPa)	Ultimate Strength (MPa)
Primitive solid	513	20	62
I-WP solid	286	10	15
Neovius solid	183	4	5

Table 5. Quantitative benchmarking of TPMS lattice performance with previous studies

Reference	Material & Process	TPMS Type	Relative Density (ρ*)	Relative Strength / Performance Order	Key Quantitative Findings
Present study	UHPFRC (Numerical)	Solid	40%	Primitive > I-WP > Neovius	Primitive yield stress (20 MPa) was 100% higher than I-WP (10 MPa) and 400% higher than Neovius (4 MPa).
Ahmed et al. [30]	AlSi10Mg Metal (SLM)	Sheet	20% - 40%	I-WP > Gyroid > Primitive	Sheet I-WP exhibited 35% higher ultimate compressive strength compared to skeletal Primitive.
Fu et al. [29]	Resin (SLA)	Solid	30%	Primitive > I-WP	Solid Primitive exhibited 39% higher compressive yield strength than solid I-WP.
Abueidda et al. [20]	PA2200 Polymer (SLS)	Sheet	10% & 24%	Neovius ≈ I-WP > Primitive	At ρ* = 24%, I-WP (5.2 MPa) and Neovius (5.1 MPa) were 50–52% stronger than Primitive (3.4 MPa).
Shevchenko et al. [31]	Polyamide / PLA (SLS/FDM)	Sheet	18%-33%	I-WP > Neovius > Primitive	I-WP and Neovius were 277% and 258% stronger than Primitive, for SLS, respectively.
Kumar et al. [32]	Photopolymer Resin (SLA)	Sheet	20%	I-WP > Neovius > Primitive	The yield strength of Sheet I-WP (1.8 MPa) was 62.5% more than Primitive (1.11 MPa) and 18.2% greater than Neovius (1.52 MPa).

Table 6. Strengthening ratios for the three TPMS topologies

Lattice	Ultimate strength/Yield strength
Primitive	3.10
I-WP	1.50
Neovius	1.25



a b c

Fig. 8. Stress concentration zones for a-Primitive, b- I-WP, and c-Neovius solid TPMS lattices

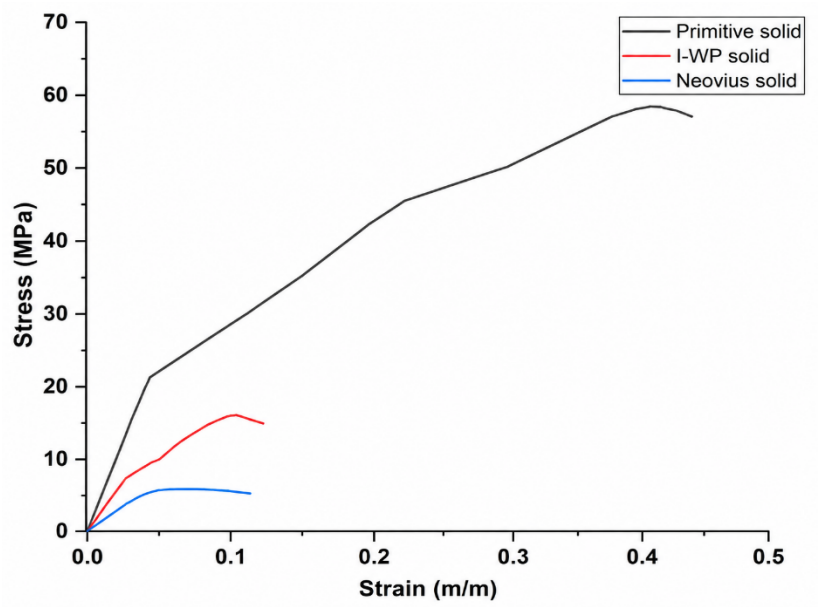


Fig. 9. Stress-strain curves of the three solid TPMS lattices

4. Limitations of the FE Simulation

It should be mentioned that the numerical methodology developed during the current research project has several limitations, even though it provides a preliminary understanding of the architecture optimization of UHPFRC lattices. The first is that the study of TPMS lattice geometries is entirely numerical. The isotropic elastoplastic behavior describes the material model, which corresponds to the second constraint. While the current continuum FE model assumes homogeneous material behavior, actual printed UHPFRC lattices may experience premature shear failure or delamination along printing interfaces before reaching the predicted theoretical ultimate strength. These manufacturing-induced interface weaknesses must be considered when translating numerical predictions into physical structural designs. In conclusion, the continuum macro-model does not take into account any local micro-cracks, the softening behavior of concrete,

or the orientation of fibers during extrusion. To overcome the limitations of homogeneous continuum modeling, future numerical work will integrate Cohesive Zone Modelling (CZM) at layer interfaces. Placing zero-thickness cohesive elements along simulated extrudate planes will enable the numerical framework to capture inter-layer debonding, progressive micro-crack propagation, and interfacial failure modes, thereby bridging the gap between ideal FE simulations and 3D-printed structural performance.

5. Conclusions

In this work, a numerical study intended to compare the compressive behavior of three UHPFRC solid TPMS lattices, including primitive, I-WP, and Neovius, is conducted at a relative density of 40%. Before the TPMS numerical simulation, the FE methodology is verified against experimental results from the literature for the compression of three 3D printed UHPFRC octet-truss lattice samples. Results from the numerical and experimental methods showed good agreement, confirming the accuracy of the adopted FE model in describing the global mechanical response of cellular UHPFRC materials. After validation, the numerical approach is applied to assess and compare the compressive behavior of the three solid TPMS lattices under uniaxial loading. It was found that the mechanical properties are highly sensitive to the choice of lattice topology. In particular, it can be shown that TPMS lattices with skeletal primitive topology exhibit the best degree of stiffness and strength among the three types of TPMS structures examined in this study. Accordingly, TPMS lattices with skeletal primitive topology exhibit the maximum strength value of up to 20 MPa, over five times greater than Neovius TPMS lattices and nearly twice as strong as I-WP TPMS lattices. Effective load transfer may be the cause of this improved performance since the lattice's vertical load channels facilitate effective load transfer. Neovius and I-WP topologies, on the other hand, are the least resistant. Nonetheless, this type of lattice structure exhibits very gentle deformation behavior, which could be useful if energy dissipation is required.

The FE analysis's assumptions of geometric perfection, homogeneous material, and the absence of defects caused some discrepancies between the numerical and experimental results, despite the relatively high correlation between the numerical and validation test results. All things considered, the results demonstrate the promise of UHPFRC solid TPMS topologies, especially the Primitive topology, for high-performance lightweight load-bearing applications in construction, providing an effective method to lower self-weight without compromising structural integrity. Overall, the results show how important topology is to the behavior of the UHPFRC TPMS lattice under compression. The numerical model's useful insights into the mechanics of load transfer and stiffness scaling in cellular UHPFRC structures may be useful for future experimental and numerical studies.

References

[1] Najm-Eddine A, Abouelmajd M, Najm-Eddine Y, Erritali I, Arroub I, Bahlaoui A, et al. Topological Optimization in 3D Concrete Printing Structures: A Review. In: 2025 11th International Conference on Optimization and Applications (ICOA). 2025. p. 1-6. https://doi.org/10.1109/ICOA66896.2025.11236952

[2] Arunothayan AR, Nematollahi B, Ranade R, Bong SH, Sanjayan J. Development of 3D-printable ultra-high performance fiber-reinforced concrete for digital construction. Constr Build Mater. 2020;257:119546. https://doi.org/10.1016/j.conbuildmat.2020.119546

[3] Arunothayan AR, Nematollahi B, Khayat KH, Ramesh A, Sanjayan JG. Rheological characterization of ultra-high performance concrete for 3D printing. Cem Concr Compos. 2023;136:104854. https://doi.org/10.1016/j.cemconcomp.2022.104854

[4] Arunothayan R, Nematollahi B, Bong SH, Ranade R, Sanjayan J. Hardened properties of 3D printable ultra-high performance fiber-reinforced concrete for digital construction applications. In: International Conference on Rheology and Processing of Construction Materials. Springer; 2019. p. 355-62. https://doi.org/10.1007/978-3-030-22566-7_41

[5] Yang Y, Wu C, Liu Z, Wang H, Ren Q. Mechanical anisotropy of ultra-high performance fiber-reinforced concrete for 3D printing. Cem Concr Compos. 2022;125:104310. https://doi.org/10.1016/j.cemconcomp.2021.104310

[6] Zhang Q, Zhang F, Medarametla SP, Li H, Zhou C, Lin D. 3D printing of graphene aerogels. Small. 2016;12(13):1702-8. https://doi.org/10.1002/smll.201503524

[7] Wang L, Jiang H, Li Z, Ma G. Mechanical behaviors of 3D printed lightweight concrete structure with hollow section. Archives of Civil and Mechanical Engineering. 2020;20. https://doi.org/10.1007/s43452-020-00017-1
[8] Graziosi S, Ballo FM, Libonati F, Senna S. 3D printing of bending-dominated soft lattices: numerical and experimental assessment. Rapid Prototyp J. 2022;28(11):51-64. https://doi.org/10.1108/RPJ-03-2022-0095
[9] Hu J, Wang S, Wang Y, Li F, Luo Z. A lightweight methodology of 3D printed objects utilizing multi-scale porous structures. Vis Comput. 2019;35:949-59. https://doi.org/10.1007/s00371-019-01672-z
[10] Chatzigeorgiou C, Piotrowski B, Chemisky Y, Laheurte P, Meraghni F. Numerical investigation of the effective mechanical properties and local stress distributions of TPMS-based and strut-based lattices for biomedical applications. J Mech Behav Biomed Mater. 2022;126:105025. https://doi.org/10.1016/j.jmbbm.2021.105025
[11] Ejeh CJ, Barsoum I, Al-Rub RKA. Flexural properties of functionally graded additively manufactured AlSi10Mg TPMS latticed-beams. Int J Mech Sci. 2022;223:107293. https://doi.org/10.1016/j.ijmecsci.2022.107293
[12] Wu Y, Li X, Li S, Wang H, Wang P, Li W. Bending behavior of additively manufactured short fiber reinforced composite sandwich structures based on triply periodic minimal surface. Polym Test. 2025;146:108779. https://doi.org/10.1016/j.polymertesting.2025.108779
[13] Mahapatra I, Velmurugan R, Jayaganthan R. Enhanced flexural performance of diamond latticed triply periodic minimal surface sandwich panels. Adv Eng Mater. 2023;2300813. https://doi.org/10.1002/adem.202300813
[14] Zhang X, Liu P, Wu L. Study on flexural properties of 3D printing functionally graded lattice structure cement composites. Mater Lett. 2024;375:137231. https://doi.org/10.1016/j.matlet.2024.137231
[15] Qiu N, Wan Y, Shen Y, Fang J. Experimental and numerical studies on mechanical properties of TPMS structures. Int J Mech Sci. 2024;261:108657. https://doi.org/10.1016/j.ijmecsci.2023.108657
[16] Chen X, Hu M, Sun Y, Yang J, Bai L, Xiong Y. Wide-range tuning of the mechanical properties of TPMS lattice structures through frequency variation. Mater Des. 2022;224:111370. https://doi.org/10.1016/j.matdes.2022.111370
[17] AlMahri S, Santiago R, Lee DW, Ramos H, Alabdouli H, Alteneiji M, et al. Evaluation of the dynamic response of triply periodic minimal surfaces under high-strain-rate compression. Addit Manuf. 2021;46:102220. https://doi.org/10.1016/j.addma.2021.102220
[18] Feng G, Li S, Xiao L, Song W. Mechanical properties and deformation behavior of functionally graded TPMS structures under static and dynamic loading. Int J Impact Eng. 2023;176:104554. https://doi.org/10.1016/j.ijimpeng.2023.104554
[19] Al-Ketan O, Lee DW, Rowshan R, Al-Rub RKA. Functionally graded and multi-morphology sheet TPMS lattices: Design, manufacturing, and mechanical properties. J Mech Behav Biomed Mater. 2020;102:103520. https://doi.org/10.1016/j.jmbbm.2019.103520
[20] Abueidda DW, Bakir M, Abu Al-Rub RK, Bergström JS, Sobh NA, Jasiuk I. Mechanical properties of 3D printed polymeric cellular materials with triply periodic minimal surface architectures. Mater Des. 2017;122:255-67. https://doi.org/10.1016/j.matdes.2017.03.018
[21] Stepinac L. Characterisation and modelling of additively manufactured polymeric tpms lattices for structural application. University of Zagreb. Faculty of Civil Engineering; 2024.
[22] Sengsri P, Fu H, Kaewunruen S. Mechanical properties and energy-absorption capability of a 3D-printed TPMS sandwich lattice model for meta-functional composite bridge bearing applications. Journal of Composites Science. 2022;6(3):71. https://doi.org/10.3390/jcs6030071
[23] Viet N V, Karathanasopoulos N, Zaki W. Mechanical attributes and wave propagation characteristics of TPMS lattice structures. Mechanics of Materials. 2022;172:104363. https://doi.org/10.1016/j.mechmat.2022.104363
[24] Kien Nguyen T, Shazwan Suhaizan M, Nguyen-Xuan H, Tran P. Mechanical responses of buoyant bio-inspired foamed concrete structures. Constr Build Mater. 2023;391:131731. https://doi.org/10.1016/j.conbuildmat.2023.131731
[25] Le BA, Tran BV, Vu TS, Nguyen QB, Nguyen HQ, Chateau X. Anisotropy and Mechanical Characteristics of Ultra-High Performance Concrete and Its Interpenetrating Phase Composite with Triply Periodic Minimal Surface Architectures. J Appl Mech. 2024;91(9):91008. https://doi.org/10.1115/1.4065901
[26] Zhao M, Li X, Zhang DZ, Zhai W. TPMS-based interpenetrating lattice structures: design, mechanical properties and multiscale optimization. Int J Mech Sci. 2023;244:108092. https://doi.org/10.1016/j.ijmecsci.2022.108092
[27] Aghdasi P, Williams ID, Salazar B, Panditi N, Taylor HK, Ostertag CP. An octet-truss-engineered concrete (OTEC) for lightweight structures. Compos Struct. 2019;207:373-84. https://doi.org/10.1016/j.compstruct.2018.09.011

[28] Simsek U, Akbulut A, Gayir CE, Basaran C, Sendur P. Modal characterization of additively manufactured TPMS structures: comparison between different modeling methods. International Journal of Advanced Manufacturing Technology. 2021;115(3):657-74. https://doi.org/10.1007/s00170-020-06174-0
[29] Fu H, Huang X, Kaewunruen S. Nonlinear instabilities of TPMS cellular units under axially loaded conditions. International Journal of Structural Stability and Dynamics. 2024;24(23):2450261. https://doi.org/10.1142/S0219455424502614
[30] Ahmed N, Barsoum I, Abu Al-Rub RK. Numerical investigation on the effect of residual stresses on the effective mechanical properties of 3D-printed TPMS lattices. Metals (Basel). 2022;12(8):1344. https://doi.org/10.3390/met12081344
[31] Shevchenko V, Balabanov S, Sychov M, Karimova L. Prediction of cellular structure mechanical properties with the geometry of triply periodic minimal surfaces (TPMS). ACS Omega. 2023;8(30):26895-905. https://doi.org/10.1021/acsomega.3c01631
[32] Kumar R, Ramkumar J, Balani K. Design and parametrization of TPMS lattice using computational and experimental approach. Engineering Research Express. 2024;6. https://doi.org/10.1088/2631-8695/ad7109